Structure–function analyses of a pertussis-like toxin from pathogenic *Escherichia coli*reveal a distinct mechanism of inhibition of trimeric G-proteins

Dene R. Littler[‡], Sheng Y. Ang[§], Danilo G. Moriel[¶], Martina Kocan[§], Oded Kleifeld[|], Matthew D. Johnson[‡], Mai T. Tran[‡], Adrienne W. Paton[**], James C. Paton[**], Roger J. Summers[§], Mark A. Schembri[¶], Jamie Rossjohn[‡,‡‡,§§] and Travis Beddoe[¶¶]

[‡]Infection and Immunity Program and Department of Biochemistry and Molecular Biology, Biomedicine Discovery Institute, Monash University, Clayton, Victoria 3800, Australia,
[§]Monash Institute of Pharmaceutical Sciences, Monash University, Parkville, Victoria 3052, Australia,
[¶]School of Chemistry and Molecular Biosciences, University of Queensland, Brisbane, Queensland 4072, Australia,
[|]Faculty of Biology, Technion-Israel Institute of Technology, Haifa 3200003, Israel,
[**]Research Centre for Infectious Diseases, School of Biological Sciences, University of Adelaide, South Australia 5005, Australia,
[‡‡]Institute of Infection and Immunity, School of Medicine, Cardiff University, Heath Park, Cardiff CF14 4XN, Wales, United Kingdom,
[§§]ARC Centre of Excellence in Advanced Molecular Imaging, Monash University, Clayton, Victoria 3800, Australia, and
[¶¶]Department of Animal, Plant and Soil Science and Centre for Agri Bioscience, La Trobe University, Bundoora, Victoria 3086, Australia

ABSTRACT

Pertussis-like toxins are secreted by several bacterial pathogens during infection. They belong to the AB_5 virulence factors, which bind to glycans on host cell membranes for internalization. Host cell recognition and internalization are mediated by toxin B subunits sharing a unique pentameric ring-like assembly. Although the role of pertussis toxin in whooping cough is well-established, pertussis-like toxins produced by other bacteria are less studied, and their mechanisms of action are unclear. Here, we report that some extra-intestinal *Escherichia coli* pathogens (*i.e.* those that reside in the gut but can spread to other bodily locations) encode a pertussis-like toxin that inhibits mammalian cell growth *in vitro*. We found that this protein, *Ec*Plt, is related to toxins produced by both nontyphoidal and typhoidal *Salmonella* serovars. Pertussis-like toxins are secreted as disulfide-bonded heterohexamers in which the catalytic ADP-ribosyltransferase subunit is activated when exposed to the reducing environment in mammalian cells. We found here that the reduced *Ec*Plt exhibits large structural rearrangements associated with its activation. We noted that inhibitory residues tethered within the NAD^+-binding site by an intramolecular disulfide in the oxidized state dissociate upon the reduction and enable loop restructuring to form the nucleotide-binding site. Surprisingly, although pertussis toxin targets a cysteine residue within the α subunit of inhibitory trimeric G-proteins, we observed that

activated *Ec*Plt toxin modifies a proximal lysine/asparagine residue instead. In conclusion, our results reveal the molecular mechanism underpinning activation of pertussis-like toxins, and we also identified differences in host target specificity.

INTRODUCTION

Pathogenic *Escherichia coli* strains preferentially inhabit different sites within their hosts, with enteric or extra-intestinal niches presenting distinctly different challenges. Infection by enteric or diarrheagenic *E. coli* can result in gastroenteritis, but it seldom spreads beyond the intestinal tract except in immunocompromised individuals (1, 2). In contrast, extra-intestinal *E. coli* (ExPEC)[7] strains such as uropathogenic *E. coli* (UPEC) or neonatal meningitis *E. coli* can reside passively within the gut until conditions permit their expansion into the urinary tract, blood, or nervous system where they may potentially cause life-threatening disease (3). To do so, ExPEC strains express a range of virulence factors, often encoded on mobile genetic elements, including AB_5 toxins. Such phage-encoded toxins are secreted by several major bacterial pathogens, including enterotoxigenic *E. coli* (55) and enterohemorrhagic *E. coli* (4); *Vibrio cholerae*(5), *Shigella* (6), *Salmonella* (7), and *Bordetella pertussis* (8, 9). Modern sequencing techniques frequently identify novel AB_5 toxins related to those previously studied, but their conservation at the level of function remains to be determined.

AB_5 virulence factors bind to glycans present on the surface of eukaryotic host cell membranes resulting in their internalization. Once inside the host cell, the enzymatic A subunits are released allowing them to disrupt host biochemistry and physiology. Host cell recognition and internalization are mediated by the toxin B subunits that share a unique pentameric ring-like assembly. This juxtaposes with the A subunit cargos that are class-specific and structurally divergent, and their activation inside mammalian cells occurs through distinct intracellular detection and release mechanisms (10). Five AB_5 toxin families currently exist: the enzymatic components of the subtilase cytotoxin (11) and EcxAB toxin (12) are proteases, whereas those of the Shiga group (6) are ribosome inhibitors; cholera and heat-labile enterotoxins (4, 5) carry related ADP-ribosyltransferases, as do the related pertussis (8, 9) and typhoid toxin (7) proteins.

Toxin ADP-ribosyltransferases (ARTs) hydrolyze the nicotinamide group from $NAD^+$and transfer the ADP-ribose moiety onto specific host proteins. Pertussis toxin specifically targets

inhibitory trimeric G-proteins by modifying a conserved cysteine located four residues from the C termini of the Gα subunit (13). This modification renders the $G\alpha_{i/o}$ subunits unable to associate with their cognate G-protein-coupled receptors (GPCRs) thus modulating the host's immune response. A series of related pertussis-like (Plt) toxins exist within the genomes of pathogenic bacteria, including strains of *E. coli*, *Salmonella*, and *Yersinia*. The bacterial strains harboring such virulence factors are diverse, and their evolutionary relationship is complicated due to the spread of these genes on mobile genetic elements. Proteins within the Plt family include the atypical archetype member whose glycan-binding B subunits have expanded and diverged within the *B. pertussis* genome to form four separate genes yielding a pseudopentameric glycan-binding platform. In contrast, other pertussis-like toxins display a homopentameric glycan-binding stoichiometry. All Plt proteins nonetheless carry a conserved catalytic A subunit.

In the secreted state, the enzymatic ART domain of pertussis-like toxins lies atop the five glycan-binding subunits allowing its C terminus to thread through a U-shaped NAD^+-binding cleft before plunging into the pore of the B subunit pentamer (7, 9). When these C-terminal residues are truncated from pertussis toxin, its ART domain is constitutively active *in vitro* but is unable to associate with its pseudopentamer or enter cells (14). Enzymatic activation *in vivo* requires proteolytic separation of the inhibitory C terminus and reduction of a connecting disulfide. Although the molecular mechanisms underlying an alternative activation mechanism of cholera toxin are understood (15), the changes that occur following activation of a pertussis-like protein have not previously been characterized.

Although the association of pertussis toxin with whooping cough is well-established, orthologous pertussis-like toxins present within other pathogenic bacterial infections are less studied, and their mechanism(s) of action are unclear (7). Here we identify a pertussis-like AB_5 protein (*Ec*PltAB) from clinical *E. coli* isolates that is related to the typhoid and ArtAB toxins observed in typhoidal and nontyphoidal *Salmonella* serovars. We provide structures that confirm that pertussis-like toxins are secreted as inactive forms in which an intramolecular disulfide holds an occluding C-terminal tail within the NAD^+-binding site. This conserved disulfide also serves as a redox switch that senses host cell entry, with reduction of the bond allowing displacement of the occluding C-terminal residues, facilitating NAD^+ binding and maturation of catalytic activity. At a global level, the existence of *Ec*PltAB-type proteins, and their relatives (55) expands the family of known bacterial

pertussis-like toxins capable of modulating the human immune system. Furthermore, we show that although AB_5 proteins are segregated into evolutionarily related enzyme families, these may not always modify the same residues within host proteins.

RESULTS

Identification of EcPltAB

The frequency with which pathogenic bacterial strains are isolated from clinical settings does not necessarily correlate with their representation in genomic databases, yet it remains a useful proxy measure. We thus determined the prevalence of genes encoding AB_5-type toxins among complete and draft *E. coli* genome sequences available on the NCBI database. *E. coli* genomes were queried using previously identified A and B subunit sequences. As expected, most genes discovered corresponded to previously known *E. coli* toxins; by far the most prevalent were the Shiga toxins produced by Shiga toxigenic *E. coli*, proteins whose action can cause hemolytic-uremic syndrome following infection, identified in 19% of genomes (supplemental Fig. S1). The next most prevalent were toxins from the cholera family LT-I and LT-II heat-labile enterotoxins secreted by enterotoxigenic *E. coli* (Fig. 1), identified in ~8% of the genomes. The properties of these enteric *E. coli* toxins are well-established (4, 5, 11). However, the third most common set of AB_5 genes identified was a series of related pertussis-like proteins found in ExPEC genomes, particularly from phylogroup B2 (Fig. 1). The B subunit of these toxins shared 69% sequence identity to *ArtB* and the upstream A subunit 70% identity to *ArtA*, two components of a pertussis-like toxin produced by *Salmonella typhimurium* DT104 (16). In contrast to these *Salmonella* and *Escherichia* orthologs, the archetype pertussis toxin has an expanded set of four glycan-binding B subunits (named S2–S5) associated with a single catalytic A or S1 subunit. The *Salmonella* ArtAB protein is an active ADP-ribosyltransferase (17), whereas a related typhoid toxin additionally serves as a cargo carrier for an accessory cytolethal distending toxin (7). Our analysis indicates that the *E. coli* Plt toxins are more evolutionarily diverse than the currently identified *Salmonella* variants, with at least three semi-separate lineages sharing between 70 and 80% sequence identity. We refer to the product of these pertussis-like genes as *E. coli*-pertussis-like toxins (*Ec*Plt).

Cytotoxicity of EcPltAB

We characterized the *Ec*Plt toxin family by cloning a number of representative members and expressing them using standard recombinant techniques, focusing primarily on the *EcPlt* genes (E9YZW8 and E9YZW9) cloned from UPEC isolate PA26B. The oxidized *Ec*PltAB holotoxin was purified after co-expressing both subunits using a periplasmic expression system (18). The 96-kDa soluble protein complex eluted on gel filtration with a molecular mass consistent with that of an AB_5 heterohexameric stoichiometry. To ascertain whether this holotoxin was functional, it was added to human embryonic kidney (HEK293T) or African green monkey kidney epithelial cells (Vero). Mammalian cell lines grown to 40–50% confluency were exposed to different concentrations of *Ec*PltAB (Fig. 2*a* and supplemental Fig. S2). The characteristic response profile of pertussis toxin involves a slow cellular entry mechanism followed by an accumulative interruption of signaling resulting in clustered growth (19). Over an 18-h period, control-treated cells remained unaffected and continued to proliferate, although those exposed to *Ec*PltAB displayed cell clustering and an absence of growth (see supplemental Fig. S2, *a–c*) compared with buffer-alone controls (supplemental Fig. S2*d*).

Next, we performed a glycan array analysis to determine the specificity of *Ec*PltAB (see supplemental Table S1). Its B subunit displayed avidity for a broad range of branched eukaryotic glycans, especially those with *N*-acetylneuraminic acid (Neu5Ac) termini, thus implying *Ec*Plt targets a similar range of cell types as typhoid toxin (7).

We next sought to establish which eukaryotic proteins were targeted by *Ec*PltA. The *Ec*PltA toxin shares 50–70% identity with *Salmonella* ArtA proteins and 31% identity with the pertussis toxin's catalytic S1 subunit, two known ADP-ribosyltransferases that modify the α subunits of inhibitory trimeric GTP-binding proteins (17, 20). We set up an assay to identify equivalent *Ec*PltA substrates by using biotin-conjugated NAD^+ as substrate for the toxins. In such assays, ADP-ribosylation also adds a biotin tag to protein substrates that can then be imaged by Western blotting using streptavidin-horseradish peroxidase. Holotoxin (*Ec*PltAB or PT) versions of this assay are dependent upon toxin activation and ADP-ribosylation rate, although when the assay is performed with constitutively active proteins (*Ec*PltA or PT S1), only the ADP-ribosylation rate is measured.

Using radiolabeled substrate, other groups (20) have shown that the PT holotoxin is activated by the presence of ATP and reducing agents. Our own ADP-ribosylation assay recapitulates this result with a 41-kDa band being modified by PT in crudely purified trimeric G-protein brain extracts or Vero cell lysates under identical conditions (Fig. 2). A similar band was observed in reactions containing the *Ec*PltAB holotoxin (Fig. 2). In both reactions, a major band at ~41 kDa was ADP-ribosylated and migrated close to the molecular weight of PT-treated $G\alpha_i$ proteins (Fig. 2*b*, *left panel*). To confirm that *Ec*PltA targeted $G\alpha_i$ subunits, we cloned two *Hs*$G\alpha_{i3}$ constructs (the most readily expressed isoform): the full-length protein and a more soluble construct lacking the N-terminal aliphatic helix (*Hs*$G\alpha_{i3}\Delta N$). Following expression and purification, full-length *Hs*$G\alpha_{i3}$ acted as substrate for the toxin's ADP-ribosyltransferase activity and migrated at a similar molecular weight to a band modified in Vero cell extracts, whereas other proteins within the Coomassie-stained lysate did not (Fig. 2*b*, *right panel*). Both the full-length protein and $G\alpha_{i3}$ ΔN-mutant served equally well as substrates for PT or *Ec*Plt (supplemental Fig. S3), the latter $G\alpha_{i3}\Delta N$ construct was favored for routine assays due to its enhanced stability.

PT is responsible for many of the pathogenic features of *B. pertussis*. However, other *Bordetella* species also contain *ptx*-like genes yet fail to produce the toxin because of inactive promoters (21). Using our assay, we sought to identify whether ADP-ribosyltransferase activity was detectable in the supernatant of UPEC strain PA26B. UPEC PA26B was cultured in the presence of prophage-inducing agents. After 12 h of growth, bacterial cells were removed by filtration, and the supernatant was tested for ADP-ribosyltransferase activity using *Hs*$G\alpha_{i3}\Delta N$ as a substrate. In control reactions employing purified *Ec*PltAB, a robust ADP-ribosyltransferase response was observed using 20 nM pure toxin (Fig. 2*c, 1st lane*). Prior to commencing the reaction, the supernatant of PA26B cells was seen to contain a natively biotinylated 20-kDa protein, but this was readily distinguishable from our host *Hs*$G\alpha_{i3}\Delta N$ target (Fig. 2*c, 2nd lane*). When *Hs*$G\alpha_{i3}\Delta N$ was added to the filtered supernatant of PA26B, we observed ADP-ribosylation of the substrate (Fig. 2*c, 3rd lane*) suggesting, but not conclusively proving, that *Ec*PltAB is actively expressed.

The B subunit of the typhoid toxin impacts cell-signaling pathways independent of its associated catalytic A subunits (22). To determine whether the growth-arrest phenotype induced by *Ec*PltAB resulted from its enzymatic activity, inactivating mutations were

incorporated into the A subunit. A highly conserved (Q/E)*X*E motif is present in many ADP-ribosyltransferases and is essential for activity (23) (residues ^{116}QNE^{118} in *Ec*PltA). Mutation of residue Glu-118 to an aspartic acid residue resulted in a requirement for 1000-fold higher concentrations of toxin to induce the same level of growth arrest as wild-type *Ec*PltAB toxin (Fig. 2*d*). Furthermore, a Q116D,E118D double mutant that retains a wild-type B subunit showed no effect on growth and was indistinguishable from control reactions even at 50 μg/ml toxin (Fig. 2*d* and supplemental Fig. S2*e*), and as discussed later, this mutant displayed no discernible enzymatic activity (Fig. 7*c*). *Ec*PltAB thus appears to be expressed by ExPEC, and its ADP-ribosyltransferase activity is cytotoxic to mammalian cells.

The presence of ATP, phosphate, and detergent assists with activation of the PT S1 subunit by promoting dissociation from its pseudopentamer and increasing its exposure to the local microenvironment (24). ATP binds within the central pseudopentameric pore of the pertussis toxin, destabilizing the quaternary structure (25). We sought to determine whether the activation requirements for the EcPltAB toxin were similar. Our assay recapitulated the finding that reducing agents activate PT and that this process is synergistically enhanced by the presence of ATP (Fig. 3a, 1st to 5th lanes). Like PT, the EcPltAB holotoxin is inactive when oxidized, and higher concentrations of reducing agent result in increased catalytic activity in vitro (Fig. 3a, 6th to 8th lanes). However, ATP did not synergistically enhance this process (in Fig. 3a, 4th lane is 95% more intense than 2nd lane, although the intensities of the 7th and 9th lanes are within 1%). The ATP-binding site of the PT pseudopentamer appears absent within the homopentameric EcPltAB. We examined whether the nature of the reducing agent affected EcPltAB activation by repeating the ADP-ribosylation assays in the presence of intracellular (2 mM) or serum (2 μM) concentrations of glutathione using different redox ratios. Reduced glutathione alone was ~20% more effective at inducing toxin activation in vitro than an equivalent concentration of TCEP (Fig. 3c), yet even small quantities of oxidized glutathione (GSSG) drastically slowed activation. Thus, although some characteristics are shared, the sequence divergence that exists between pertussis toxin and pertussis-like toxins results in differences in their respective activation mechanisms.

Protein substrates

PT targets the α subunits of human inhibitory trimeric G-proteins by transferring the ADP-ribose moiety of NAD+ onto a conserved cysteine four residues from their C termini. PT-sensitive substrates primarily belong to the heterotrimeric Gi/Go protein subfamily, which in

humans includes the 40.5-kDa proteins Gαi1, Gαi2, Gαi3, and Gαio, as well as the equivalent subunit from transducin. The Salmonella ArtA pertussis-like toxin modifies this same set of proteins (17), indicating some degree of target conservation. As the HsGαi3 was shown to be an EcPltA substrate, we sought to test for activity against the remaining trimeric Gi proteins enriched from brain lysate using equal amounts of a commercial Gβ-immunoprecipitated source of trimeric inhibitor G-proteins. Mammalian inhibitory Gαi proteins possess similar molecular weights but have divergent pI values (Gαi2/Gαo (5.34), Gαi3 (5.50), and Gαi1 (5.7)), allowing for their separation as three distinct bands on an isoelectric focusing gel. PT-catalyzed ADP-ribosylation of brain lysate (Fig. 3c, left panel) showed three distinguishable IEF bands, roughly reproducing its substrate preference of Gαi2/Gαo > Gαi3 > Gαi1 (17). In contrast, when the same experiment was performed using EcPltA, at least three subunits were modified, with a slight relative preference for Gαi3 over Gαi2/Gαo and Gαi1 (Fig. 3c, right panel). EcPlt thus represents a functional AB5 toxin that retains some, but not all, characteristics of the archetypical PT.

Protein substrate ADP – ribosylation site

Pertussis toxin specifically modifies a conserved cysteine four amino acids from the C terminus of Gαi/o subunits (26) (Cys-351) and in doing so renders them unable to interact with their cognate receptors (Fig. 4a). In our ADP-ribosyltransferase assay, and as reported by others (27), C351S mutations within the Gαi/o proteins leave them resistant to PT modification but surprisingly no modification by EcPltA (see Fig. 4b). To determine whether EcPltA targeted another cysteine residue, we mutated each cysteine residue and repeated the experiment; all such HsGαi3 mutants were simultaneously treated with PT as a control. As shown in Fig. 4b, all other cysteine knock-out mutants act equally well as substrates for either toxin. When cholera toxin's primary site of modification within stimulatory Gαs proteins is removed, lower affinity sites instead become targeted (28). In case EcPltA targeted more than one cysteine, we pretreated HsGαi3 with iodoacetamide for 24 h and re-purified the protein prior to the assay (Fig. 4c). Alkylating all available cysteines renders HsGαi3 resistant to PT modification as expected, but it does not prevent the protein from being a substrate for EcPltA, indicating an alternative chemical linkage. The ADP-ribosylation products produced by EcPltA and PT were not sensitive to 1 M hydroxylamine treatment suggesting the modification is on residues other than Glu and Asp. However, lysine methylation of HsGαi3 rendered it entirely resistant to EcPltA modification (Fig. 4c). PT

could still act on methylated HsGαi3 substrate but at a slightly reduced rate compared with controls (Fig. 4c).

To identify the residue(s) within HsGαi3 modified by EcPltA, the reaction product was subjected to MS-MS analysis. ADP-ribosylation results in a +541-Da mass shift to precursor peptides, and fragmentation of the pyrophosphate bond also liberates a characteristic 348.1-Da adenine monophosphate during product ion scans (supplemental Fig. S4). We obtained full peptide coverage of HsGαi3 and could not detect any evidence of cysteine modification, instead ADP-ribosylated modification sites were identified in HsGαi3 C-terminal sequences: 331NVQFVFDAVTDVII-K(ADP-ribosylated)-NNLK349 and 346NN-(ADP-ribosylated)-LKECGLY354. Thus, EcPltA ADP-ribosylates two residues (Lys-345 and Asn-347) at the C terminus of HsGαi3, sites distinct from PT modification of Cys-351. We next constructed three mutants, HsGαi3(K345A), HsGαi3(N346A), and HsGαi3(N347A), and tested their suitability as substrates for both toxins. HsGαi3(K345A) was seen to be resistant to ADP-ribosylation by EcPltA, yet it was readily modified by the constitutively active PT S1 (Fig. 4d); HsGαi3(N346A) was readily ADP-ribosylated by either toxin and HsGαi3(N347A) by neither toxin (Fig. 4e). It is noteworthy that mutation of either Lys-345 or Asn-347 to alanine also reduced enzymatic activity against the other site, suggesting a concerted mechanism of recognition. Together, these experiments suggest that different pertussis-like toxins can target distinct but nearby residues within the C termini of Gαiproteins.

$G\alpha_{i/o}$ recruitment to GPCRs is disrupted by EcPltAB

We next examined what effect EcPltAB had on GPCR-signaling pathways in cells. The Relaxin family peptide 4 receptor (RXFP4) is a GPCR that recruits Gαi/o subunits upon binding its ligand: insulin-like peptide 5 (INSL5); the induced nucleotide exchange inhibits forskolin-stimulated cAMP production and promotes ERK phosphorylation (29), a response that can be abolished through PT pretreatment. Gαi/o proteins with a C351I mutation (mGαoA, mGαoB, mGαi1, mGαi2, or mGαi3) are PT-insensitive and can be used to rescue the PT-abolished INSL5-stimulated ERK1/2 response to determine which Gαi/o subunits are recruited to RXFP4. We first confirmed that PT could completely abrogate the INSL5-stimulated ERK1/2 response within Chinese hamster ovary (CHO)-RXFP4 cells transfected with the pcDNA3 vector control (Fig. 5a); an identical result was obtained with EcPltAB pretreatment (Fig. 5a). Next, we demonstrated that ERK1/2 responses were partially restored in PT-treated cells transfected with mGαoA, mGαoB, mGαi2, and to a smaller extent with

mGαi3 but negligibly with Gαi1 (Fig. 5, b–f). GPCR RXFP4 can thus recruit all isoforms of Gαi/o, although it does so in a preferential manner, predominantly recruiting GαoA = GαoB = Gαi2 > Gαi3 ≥ Gαi1. None of the PT-insensitive Gαi/o mutants tested were able to restore INSL5-stimulated ERK1/2 responses in cells treated with EcPltAB (Fig. 5, b–f), underlining that within cells the residue(s) on Gαi/o targeted by EcPltAB differ from the canonical Cys-351 ADP-ribosylated by PT and that once modified the GPCR signaling is disrupted.

As Gαi/o subunits carrying the PT-resistant C351I mutant remain sensitive to EcPltAB treatment, we next sought to identify alternative EcPlt-resistant mutations. To do so we monitored the cAMP concentration in cells responding to the adenylyl cyclase activator forskolin (supplemental Fig. S5a). This stimulatory response can be counteracted by inhibitory trimeric G-proteins coupled to INSL5-induced RXFP4 signaling, which acts to restore cAMP levels to a near basal state (supplemental Fig. S5a). The RXFP4-transduced inhibitory signal can be abrogated by either toxin (supplemental Fig. S5a), and reconstituting C351I Gαi/o subunits allows partial recovery of the inhibitory signal in the presence of PT (supplemental Fig. S5, b–f) but not EcPltAB. In an attempt to achieve an equivalent response for the enterobacterial toxin, we mutated its two identified ADP-ribosylation sites within HsGαi3 to alanine (N347A and K345A) and repeated the experiment (supplemental Fig. S5, g and h). Neither HsGαi3(N347A) nor HsGαi3(K345A) facilitated the recovery of PT-treated cells. In contrast, EcPltAB treatment of cells transfected with HsGαi3(N347A) displayed a 26 ± 5% difference in the cAMP response in the presence of INSL5/forskolin or forskolin alone (supplemental Fig. S5g), consistent with the N347A mutant providing a degree of protection for EcPltAB but not for PT. In the same experiment, HsGαi3(K345A) did not obviously allow recovery of INSL5-mediated signaling (Fig. 7h).

Structure of the secreted EcPltAB holotoxin

To understand the secreted ExPEC toxins in more detail, we determined the 2.4 Å crystal structure of the EcPltAB holotoxin (see supplemental Methods and Table 1 for details). This heterohexameric complex resembles a blunted pyramid in which the EcPltA subunit sits atop a pentameric B subunit base, thereby adopting an overall quaternary structure of the AB5 family (Fig. 6a). In the secreted oxidized state, the enzymatic A subunit contains a single intramolecular disulfide bond between the two conserved cysteines (Cys-41 and Cys-192, Fig. 6b); each of the five EcPltB subunits contains a further two intramolecular

disulfides. EcPltA shares 52% sequence identity to the typhoid toxin's A subunit (30) and 31% identity to the S1 subunit of pertussis toxin (9), its two closest known structural homologs (root mean squared deviation of 1.1 Å over 207 of 224 Cα; and 2.0 Å over 186 Cα, respectively PDBeFOLD). In all three holotoxins, the respective orientation of the A subunit atop the B pentamer is similar, with the Cα backbone structure of the EcPlt holotoxin and the lower AB5 section of the typhoid toxin overlaying over most of their length. The conserved intramolecular disulfide of pertussis group toxins holds their inhibitory C-terminal residues inside their nucleotide-binding sites (Fig. 6b), preventing catalytic activity prior to entry into the reducing environment of the host cytoplasm.

Structure of the cytoplasmic NAD^+-bound EcPltA

To determine what structural changes occur following release of the C-terminal redox switch, we determined a 1.8-Å resolution structure of the constitutively active catalytic EcPltA subunit (residues 5–181) purified under reducing conditions (Table 1). As ART enzymes display off-target NAD+-glycohydrolase activity in the absence of substrate, we utilized the catalytically inactive mutant (Q116D,E118D) to slow this reaction and permit stable co-complex formation with the NAD+ substrate (30). These crystals diffracted in space group P1 with four complexes of NAD+–EcPltAcat within the asymmetric unit allowing independent models of the ART domain to be compared. The enzymatic core of the ART fold consists of ~150 amino acids and has a U-shape with a concave cleft creating the NAD+-binding site (Fig. 6c). The two β-sheets of EcPltA are on either side of this nucleotide-binding cleft: on one side is the β-sheet with strands s1, s3, s6, and s7 sandwiched between helix 3 and helix 1, and on the other side is the fold's smaller s2, s5, and s4 β-sheet along with its h2, h4, and h5 helices. Unbiased omit maps showed NAD+ to be bound inside the U-shaped ART domain with two distinct binding modes observed, one extended and the other semi-extended (Fig. 7) (31). The extended conformation (supplemental Fig. S6a) dominates in the A, B, and C protomers and the semi-extended conformation in D (supplemental Fig. S6b). Both bound forms of NAD+ adopt highly folded nicotinamide mononucleotide (NMN) sections, whereas the adenine base transits between alternative aromatic stacking interactions. The common factor within the two distinct nucleotide conformations is the folded NMN group, and forcing the nucleotide to adopt this form is proposed to be an integral part of catalysis (32). The residues stabilizing the compact NMN are contributed from both sides of the binding cleft. Strand s1 provides a conserved phosphate-binding nucleophilic amino acid (Arg-9) also found in PT, although the amide group of the nicotinamide moiety forms hydrogen bonds to

the peptide backbone (Fig. 7a). On the other side of the cleft, residues within a semi-conserved “STS” motif within the s2 strand position the scissile bond for catalysis by clasping the nicotinic ring of NAD+ (actual residues 52ATT54, supplemental Fig. S6c). The inactivating E118D mutation of the catalytically essential glutamate shifts the negatively charged carboxyl away from the nucleotide (Fig. 7, a and b); if the Glu-118 rotamer observed in the wild-type holotoxin was to be maintained following reduction, its carboxyl group would be positioned within hydrogen-bonding distance of the N-ribose's 2′-hydroxyl (Fig. 7e). This interaction is highly conserved within ART enzymes and is thought to promote nicotinamide scission by stabilizing the formation of an oxocarbenium ion intermediate (33). The movement of the carboxyl group caused by the E118D mutation helps explain why this otherwise relatively conservative substitution is inactivating in the ART enzymes (Fig. 7c).

In the extended NAD+ conformation, the adenine base interleaves between the guanidinium group of Arg-13 and the indole ring of His-26. A similar interleaved interaction is seen in the NAD+-bound cholera toxin structure (15). In contrast, the semi-extended NAD+ conformation has the adenine base stacked atop Tyr-67 (Fig. 7b). The Y67A mutation was seen to abrogate catalytic activity in the ADP-ribosyltransferase assays using HsGαi3 as substrate (Fig. 7c), but ~25% wild-type activity is retained by Y67F mutants suggesting it is the aromatic base-stacking role that is its more vital feature (Fig. 7c). Moreover, an S70W mutation, which would disrupt the adenosine-binding site of the semi-extended but not the extended conformation, also displayed minimal ADP-ribosyltransferase activity in vitro (Fig. 7, band c) suggesting this conformation may play a role during catalysis.

Several EcPltA residues located at the intersubunit interface of the holotoxin become solvent-exposed following subunit dissociation; this includes Ile-111 on h5 and Ile-58 and Ser-56 on h3 (gray labels in Fig. 7b). To determine whether any such residues are also involved in protein interactions with the transfer target, they were mutated to large bulky residues to disrupt potential recognition interfaces. All mutations on the exterior face of h3 had no effect (Fig. 7c), whereas equivalent mutations on h5 (I111Y) were inactivating. This h5 helix is N-terminal to the catalytic (E/Q)XE motif, a region of the ART domain that in cholera and C3-like toxins corresponds to a conserved flexible loop between strands s4 and s5 known to be necessary for substrate recognition (34).

Redox-induced structural changes

We compared the inactive oxidized and active NAD+-bound states of EcPltA (Fig. 7e; supplemental movie). This shows that the activation mechanism of pertussis-like toxins is fundamentally different from the loop-refolding mechanism of cholera toxin (15). The conserved intramolecular disulfide within the EcPltA-oxidized state (Cys-41–Cys-192) is located inside the NAD+-binding cleft directly above the catalytic glutamate (Glu-118), Cys-192 being the C-terminal residue of the short inhibitory A2 helix. In the holotoxin, the binding pocket for the nicotinamide ring is filled by Phe-193 from hA2 (Fig. 7d); subsequent A2 backbone residues then rise to thread through the cleft with Arg-199 and Arg-200 occupying the same site as the adenosine ring in the extended conformation (pink loop in Fig. 7d). The A2 loop subsequently doubles back on itself before entering the pentamer pore; during this descent, it blocks the adenosine-binding site near helix 3 for the semi-extended conformation (Fig. 7b). The nucleotide-binding site of EcPltA is made from dynamic regions of the protein that move following release of the inhibitory C-terminal residues as well as regions that remain stationary. A static floor capable of accommodating either NAD+ or the A2 peptide includes the adenine base-interleaving residues Arg-13 and His-26 (Fig. 7a), the phosphate-binding nucleophile Arg-9, and the nicotinamide "STS" clasp equivalent residues. In contrast, structural movements are required to form the side walls of the NAD+-binding site. This is necessary as the occluding C-terminal helix is more bulky than the substrate nucleotide.

After the redox-sensing disulfide is reduced, Cys-41 and the remainder of the active-site loop undergo an ~2.5-Å rigid-body inward movement toward the adenosine ribose and phosphate (Fig. 7e). This loop movement carries the h2 helix with it until it abuts the 3′-hydroxyl of the N-ribose, and in doing so the catalytic residue His-35 (35) is shifted toward the scissile N-glycosidic bond (Fig. 7, a and e) where it may interact with Glu-118. Following NAD+ binding, helix 3 pivots about its N terminus resulting in a maximal displacement from the oxidized form of ~8.2 Å (Fig. 7e). This movement allows the side chains of Tyr-67 and Ile-63 to move in and neighbor the nicotinamide ring. These NAD+-binding associated movements are likely to be conserved features of activation within typhoid toxin and pertussis toxin.

DISCUSSION

We provide the structural details of the E. coli pertussis-like toxin in its intracellular reduced form, detailing different substrate-binding modes and the redox-induced structural changes that occur during activation. In the oxidized state, the disulfide-linked C terminus of the A subunit inactivates the protein by occluding the NAD+-binding site (Fig. 6), a mechanism clearly conserved within pertussis toxin as suggested by modeling studies (36). Loss of the inhibitory A2 domain from within the nucleotide-binding cleft allows significant lobe closure and reorganization of residues about NAD+particularly within helices h2, h3, and the active-site loop. This contrasts with the activation mechanism of the cholera toxin whose A2 domain is largely external to the catalytic cleft and requires no lobe movements upon activation, but it involves significant loop restructuring (30). Our high-resolution co-crystal structure details NAD+ binding in two distinct conformations: the dominant extended conformation is similar to that observed in nucleotide-soaked CT crystals (30), and a second lower-occupancy semi-extended conformation also exists and may play a role during catalysis as C-terminal h3 mutations predicted to disrupt the base-stacked adenine abrogate activity.

The residues within h2 are relatively well-conserved, suggesting the redox-induced movement of this structural element and the restructuring of the preceding active-site loop are a conserved features of pertussis-like proteins. In contrast, helices h3 and h5 show more significant structural divergence between the pertussis and the enterobacterial holotoxins, with these regions more likely involved in binding to the transfer target. GPCR binding is disrupted by pertussis toxin through modification of the Gαi residue Cys-351, and the toxin is highly specific and unable to modify mutants lacking this residue (Fig. 6). The extent to which pertussis-like toxins are conserved could have correlated with conservation of target chemistry, yet we show EcPlt does not modify cysteine residues within Gαi proteins but instead a lysine and asparagine several residues away. Moreover, our cAMP experiments confirmed that EcPltAB enters cells and inhibits the action of Gαi proteins via a residue other than Cys-351 (Fig. 4). This is not unprecedented; human poly(ADP-ribose) polymerase 1 initiates polymer formation on C-terminal chromatin lysines (37), but ADP-ribosylation at such sites has not previously been described within bacterial toxins nor in human Gα subunits. Why would this site be targeted? GPCR:Gα-protein coupling occurs when the predominantly helical C terminus of the Gα subunit inserts into a pocket built from the cytoplasmic facing ends of the receptor TM helices. The co-complex structure of opsin in complex with the C terminus of transducin (38) shows that Cys-351 penetrates deep into the binding pocket, highlighting why pertussis toxin's modification would be incompatible with

receptor coupling. As the C terminus of receptor-bound Gα subunits are predominantly helical, Asn-347 lies a turn beneath Cys-351 interacting with the same transmembrane helix (TM3). Lys-345 is on the opposing side of the G-protein's C terminus interfacing with TM6. Thus, both Asn-347 and Lys-345 reside closer to the cytoplasmic “mouth” of the receptor's binding pocket than Cys-351 when coupled to their cognate GPCRs.

EcPltA-catalyzed ADP-ribosylation may thus block receptor recruitment of inhibitory heterotrimeric G-proteins using a related but distinct mechanism to that used by pertussis toxin. Our attempts to create an EcPlt-resistant Gαi3 subunit were partially successful (supplemental Fig. S5) and could be interpreted as indicating that the Asn-347 modification may dominate over the Lys-345 site in vivo. In vitro, both Lys-345 and Asn-347 were required for EcPltA to modify HsGαi3, so both residues may be involved in toxin:G-protein binding. Peptides consisting of the 10–20 C-terminal residues of HsGαi3 can act as minimal pertussis toxin substrate inhibitors (39) suggesting the entire protein is not necessarily required for recognition. Our work might imply that EcPlt has shifted its respective recognition motif within Gαi proteins several residues downstream from that of PT with Asn-347 playing distinct roles in both EcPlt and PT toxins recognition interfaces; we note that Asn-347 appears to be more essential for the action of EcPlt as its mutation did not provide sufficient protection to reconstitute signaling in the presence of PT. Further work will be required to validate our reconstitution experiments; mutants that disrupt the toxin–G-protein interface may also influence GPCR binding and/or GTPase activity.

Finally, pertussis toxin has become a valuable tool for dissecting GPCR pathways, and the identification of an expanded toolset of pertussis-like proteins with varied inhibitory mechanisms may permit additional experiments to be performed. Given the proven utility of PT in this role, it may be beneficial to further characterize the behavior of other pertussis-like toxins in reconstituted systems to fully understand how this toolset functions.

EXPERIMENTAL PROCEDURES

Materials

All chemicals were purchased from Sigma unless otherwise stated. Mouse INSL5 was synthesized and purified at The Florey Institute of Neuroscience and Mental Health (Melbourne, Australia) by Dr. Akhter Hossain (40). FBS, DMEM Ham's/F-12, Lipofectamine

2000, and PT were all from Life Technologies, Inc. AlphaScreen SureFire® ERK1/2 phosphorylation kits, acceptor beads, and donor beads were all from PerkinElmer Life Sciences.

Bioinformatic analysis and bacterial strains

E. coli strains containing AB5-type toxin-like genes were identified from an E. colidataset (EcoDS) comprising 1700 genome sequenced strains deposited in the NCBI database up to January 2014 (56), using a querying dataset based on characterized AB5toxins (Art (16), Shiga (41), subtilase (42), and cholera (43) toxins). Sequence comparisons were performed using the FASTA36 package (44); ORFs with an amino acid sequence identity >75% of the toxin subunits were extracted from the public dataset. A neighbor-joining tree was generated using the concatenated AB toxin subunits with ClustalW (45). The phylogenetic group was determined using an in silicotriplex scheme (46, 47), and MLST analysis was performed according to a seven-gene scheme described previously (48). UPEC strain PA26B was isolated from a patient presenting with a urinary tract infection at the Princess Alexandra Hospital (Brisbane, Australia) (54).

Toxin expression

Toxin expression was induced by stressing PA26B cells and a control K12 laboratory strain, and overnight cultures grown at 37 °C were diluted 1:40 into 40 ml of LB broth without antibiotics and grown for 4 h at 37 °C before addition of mitomycin C or 10 mMH2O2. After 24 h of growth, all proteins secreted into the media were harvested and clarified by passing through a 0.2-μm filter. 10 nM bovine catalase was added to the supernatant of cells stressed by H2O2.

Cytotoxicity assay

Kidney epithelial cells from the African green monkey (Vero cells) or human embryonic kidney (HEK293T) were expanded to 40–50% confluency in 10-cm2 dishes covered with 2 ml of Dulbecco's modified Eagle's medium supplemented with 10% (v/v) fetal calf serum. Cytotoxicity assays were performed by adding recombinant EcPltAB holotoxins at 50 μg/ml to 500 pg/ml. Cells were left for 18 h and then stained with crystal violet and imaged. The surface area covered by the cells was determined by the number of blue pixels within each image normalized against buffer controls.

Cloning

A co-expression vector for the EcPltAB toxin was created as in Ng et al. (12). Briefly, both the full-length EcPltA and EcPltB genes were chemically synthesized (GenScript), with the addition of restriction sites NdeI and XmaI and XbaI and XhoI flanking the EcPltA and EcPltB open reading frames, respectively. The EcPltA gene containing its native signal sequence was cloned directly into pBAD18. EcpltB was subcloned into pET-23 (Novagen) via XbaI and XhoI sites, resulting in a protein with a C-terminal poly-His tag and N-terminal PelB signal sequence; this construct was used for the expression of unliganded EcPltB pentamer. To produce the co-expression vector for EcPltAB, the ribosome-binding site and EcPltB was excised from pET-23 using the XbaI and HindIII restriction sites prior to being cloned downstream of EcPltA within the pBAD vector.

The catalytic domain of the pertussis toxins S1 subunit, EcPltA, and human HsGαi3proteins were cloned into a pET28 expression vector fused to a hexahistidine tag through a human rhinovirus 3C cleavage site. The constitutively active EcPltA construct encompassed residues 5–181. The HsGαi3 constructs encompassed residues 034-354 or 005-354. Mutants used in enzymatic assays were created by oligonucleotide-directed mutagenesis followed by DpnI digestion of the parental vector, with all resulting constructs confirmed by sequencing.

Protein expression and purification

For protein expression, EcPltAB was transformed into E. coli BL21(DE3) cells and then grown in LB at 37 °C containing 100 μg/ml ampicillin to A600 = 0.6 followed by a 4-h induction at 37 °C with 0.2% L-arabinose. Cell culture pellet was collected and resuspended in HEPES-buffered saline (HBS) (20 mM HEPES, pH 7.0, 150 mM NaCl) and stored at −20 °C. The cell pellet was thawed, lysed, and centrifuged with the supernatant collected and loaded onto 5 ml of nickel-Sepharose beads (GE Healthcare), equilibrated in 50 mM HEPES, pH 7.0, 250 mM NaCl, 60 mM imidazole. Unbound material was removed by washing with the same buffer. Protein was eluted with 1 M imidazole buffer (20 mM HEPES, pH 7.0, 250 mM NaCl, 1 M imidazole), with 5-ml fractions collected. Fractions containing EcPltAB were pooled, buffer-exchanged into HBS, and loaded on a Superdex S200 16/60 gel filtration column (GE Healthcare) where it eluted with a molecular mass consistent with that of a heterohexamer (~100 kDa).

Protein expression of EcPltA constructs were performed in BL21 (DE3) E. coli cells that were grown at 37 °C in LB medium supplemented with 30 μg/ml kanamycin. After reaching an A600 nm of 0.6–0.8, the temperature was dropped to 18 °C, and the cells were induced for 18 h with 0.2 mM isopropyl β-D-1-thiogalactopyranoside. Cells were harvested and resuspended in HBS with 20 mM imidazole and 1 mM TCEP, then lysed by adding 1 mg/ml lysozyme and DNase, and then sonicated. Cleared lysate was applied to a Ni-NTA affinity column and washed extensively before eluting in 20 mMHEPES, pH 7.0, 250 mM NaCl, 400 mM imidazole, 1 mM TCEP. The protein's hexahistidine tag was cleaved by incubating the eluted protein with 0.1 mg/ml GST-fused HRV 3C overnight at 4 °C. The HRV 3C protease was removed by passing over 0.1 ml of GSH-agarose resin with the flow-through subsequently purified by gel filtration on a Superdex S75 16/60 (GE Healthcare). The constructs eluted as a single peak corresponding to monomeric EcPltA. The pertussis toxin's catalytic S1 domain was purified using a similar manner.

Expression of the different HsGαi3 constructs was identical to that of EcPltA except they required 0.01% (v/v) Triton X-100 during HRV 3C cleavage, and the protein was buffer-exchanged into 20 mM HEPES, 50 mM NaCl, 1 mM TCEP to allow HiTrap Q purification prior to gel filtration. When HsGαi3 mutants were being purified for enzymatic assays, chromatographic systems and columns were purged with two intervening dummy runs: one of 0.5 M NaOH followed by 1 M HEPES, pH 7.0. When required, HsGαi3ΔN was methylated using a reductive alkylation kit (Hampton Research HR2-434) or carbamidomethylated with iodoacetamide (Pierce 90034) according to the manufacturer's instructions prior to the ion-exchange column during purification.

Enzymatic assay

Activity assays were performed using 6-Biotin-17-NAD+ (BPS Biosciences 80610) as a substrate for the modification of different G-protein substrates. The resulting biotin adducts were visualized using streptactin-conjugated horseradish peroxidase (Bio-Rad 161-0381). Briefly each reaction mix contained ~1 μM protein substrate, which consisted of recombinant HsGαi3, purified trimeric bovine brain G-proteins (EMD Millipore 371739), or whole Vero cell lysate. Standard assay conditions consisted of ~1 μM G-protein in 20 mM HEPES, pH 7.0, 140 mM NaCl, 5 mM TCEP, and 10 μM biotin-NAD+, which was incubated for 5 min at 37 °C with 20 nM toxin. Holotoxin assays were performed with up to 100 mM TCEP to induce activation and consisted of PT purified from Bordetella lysate

(Sigma P7208) or recombinant EcPltAB. Reactions were stopped by adding SDS-loading buffer and heating at 100 °C for 5 min before analysis by SDS-PAGE. Analysis by 2D gel electrophoresis was done by the Proteomics Facility, Monash University; samples were separated in the 1st dimension over broad PIG pH strip (pH 3–10) before separation in the second dimension by SDS-PAGE (gradient of 9–16% acrylamide). 1D and 2D gels were processed for analysis by Western blot; proteins were transferred to a membrane prior to being visualized using streptactin-HRP and Pierce chemiluminescence substrate. Assays performed with recombinantly produced G-proteins were subsequently stained by Coomassie to ensure equal loading. All assays were repeated three times to ensure reproducibility. Densitometry was performed using an Epson V700 scanner and data quantification via ImageQuant.

Crystallization data collection and structure determination

The EcPltAB holotoxin crystals were obtained by setting up 1:1 ratio hanging drop experiments with 16 mg/ml protein over a reservoir of 0.2 M MgCl2, 0.1 M Tris-HCl, pH 8.5, 15% (w/v) polyethylene glycol 3350 at 293 K; crystals took 2–3 weeks to grew and were then harvested by flash-freezing in liquid nitrogen after soaking in a cryoprotectant solution containing an additional 25% (v/v) glycerol prior to data collection. EcPltAB crystals diffracted to 2.35 Å in space group P65 with one heterohexamer in the asymmetric unit, and initial maps were generated using the lower AB5 section of the typhoid toxin (7) as a molecular replacement model (49) in the program Phaser (50). The resulting electron density allowed rounds of manual building and refinement using the programs COOT (51) and PHENIX (49). Because of the moderate resolution, NCS constraints were maintained throughout refinement, as releasing restraints did not result in significant improvements in Rfree. The final model encompasses residues 1–114 across all five protomer B subunits and residues 4–226 in the A subunit.

The reduced EcPltA(Q116D,E118D) mutant at 6–8 mg/ml was complexed with 20 mMNAD+ for 30 min before setting up in hanging drop crystallization experiments using a 1:1 ratio at 277 K. Clusters of plate-like crystals grew within 2–3 days over reservoirs containing 4–7% (v/v) polyethylene glycol, 0.1 M Tris, pH 8.5, and 150 mM Li2SO4. Crystals clusters were broken into single pieces prior to freezing in a reservoir complemented with 25% (v/v) glycerol and flash-frozen in liquid nitrogen, subsequently diffracting in a monoclinic space group to 1.8 Å with four molecules in the asymmetric unit. A molecular

replacement solution was obtained using a trimmed version of the holotoxin's A1 subunit as a model with four molecules found within the asymmetric unit. In protomers A–D, clear electron density was observed for residues 4–174, and there were few differences in the Cα backbone structure among protomers except for a shift in protomer D within the loop C-terminal to h3. The final model contains four NAD+ molecules and all but the C-terminal residue of the construct.

Data completeness for the EcPltA in space group P1 was a little lower than ideal. When PT or EcEPlt dissociates from their B subunits, they mimic unfolded proteins to translocate toward the cytosol. In such structures h5 is highly flexible so crystals often grew as oddly shaped clusters that needed to be fragmented. In the four molecules in the asymmetric unit, the h5 loop adopts different forms; moreover, such conformations varied when data were collected at different points in the crystal. This structural complexity caused issues for merging of datasets, and crystals showed some radiation damage after 150–200°, and the dataset was collected from multiple points on a single crystal.

Glycan array analysis

Purified EcPltAB protein at 1 or 100 μg/ml was applied to a PA_v51 glycan microarray at the Consortium of Functional Glycomics Protein–Glycan Interaction Core at Emory University, and binding was detected using Alexa488-conjugated anti-hexahistidine antibody. The data are reported as average relative fluorescence units of four of six replicates (after removal of the highest and lowest values) for each glycan represented on the array.

Mass spectrometry analysis

HsGαi3 at 2 mg/ml was treated for 1 h with a 100:1 molar ratio of EcPltA in 20 mMHEPES, 150 mM NaCl, 2.5 mM NAD+, 0.5 mM TCEP, pH 7.5. After the reaction, the protein was diluted into 20 mM HEPES, 50 mM NaCl and then bound to a HiTrap Q column and eluted under a 20-ml gradient to 1 M NaCl to remove unreacted NAD+. The reaction product was diluted into 100 mM (NH4)HCO3 and heated to 95 °C for 5 min; after cooling to room temperature, the sample was divided in two with fresh chloroacetamide added to one fraction at a final concentration of 5 mM for 30 min. Trypsin was then added at a 1:50 ratio with the digestion allowed to proceed for 18 h at 37 °C, and the digestion was finally quenched with formic acid at a final concentration of 0.25% (v/v). The resulting peptides were analyzed by

LC-MS/MS using the QExactive mass spectrometer (Thermo Fisher Scientific, Bremen, Germany) coupled on line with an RSLC nano-HPLC (Ultimate 3000, Thermo Fisher Scientific) (52). MS/MS data analysis was done with MaxQuant software (build 1.5.2.8); MS data were analyzed using MaxQuant (53) searched against the human and E. coli K12 strain protein sequences taken from UniprotKB (March, 2015). ADP-ribosylation was defined as modification of a mass of 541.0611088 Da on with diagnostic peaks of 438.03699 (m8), 348.07036 (m6), 250.09346 (m3), and 136.06177 (m1) and the corresponding natural loss peaks. The search parameters include enzyme specificity of trypsin with three missed cleavages. Search parameters also allowed for cysteine carbamidomethylation, methionine oxidation, or ADP-ribosylation on cysteine, lysine, arginine, glutamate, aspartate, and asparagine. All other search parameters were set to the default settings.

Cell culture and transient transfection

CHO cells stably expressing RXFP4 (CHO-RXFP4) were a gift from Associate Professor Ross Bathgate (Florey Institute of Neuroscience and Mental Health, Melbourne, Australia). Cells were grown and maintained in 175-cm2 flasks in DMEM/F-12 medium supplemented with 5% (v/v) fetal bovine serum (FBS) at 37 °C in humidified air containing 5% CO2. cDNA constructs for G-protein α subunits (GαoA, GαoB, Gαi1, Gαi2, or Gαi3) containing the C351I mutation were from the cDNA Resource Center (Bloomsberg, PA). HsGαi3 containing K345A and N347A mutations were generated via site-directed mutagenesis using wild-type HsGαi3 pcDNA3 vector as template. HsGαi/oconstructs carrying the mutations were transiently transfected into CHO-RXFP4 cells grown on 6-well plates using Lipofectamine 2000 as per the manufacturer's protocol.

ERK1/2 phosphorylation

18 h after transfection, CHO-RXFP4 cells were trypsinized and seeded onto 96-well plates at a density of ~50,000 cells per well and incubated for 6–8 h in complete media to allow cell adhesion. Cells were then incubated with PT, EcPltAB, or control (serum-free DMEM/F-12) for 18 h before stimulation with mouse INSL5 (0.1 to 100 nM) for 5 min and then lysed. Phosphorylation of ERK1/2 (Thr-202/Tyr-204) was detected using the AlphaScreen SureFire® kit. In brief, 4 µl of cell lysates was added to a white 384-well microplate (ProxiPlate; PerkinElmer Life Sciences) containing 5 µl of acceptor bead mix (40 parts reaction buffer/10 parts activation buffer/1 part protein A acceptor beads) and incubated for 2

h at 23 °C. Then, 2 µl of donor bead mix (20 parts dilution buffer/1 part streptavidin-coated donor beads) was added and incubated for 2 h at 23 °C. All additions and incubations were carried out under low light conditions to avoid photobleaching. Fluorescence readings were made using the Envision multilabel plate reader (PerkinElmer Life Sciences; excitation = 680 nm; emission = 520–620 nm). ERK1/2 phosphorylation is expressed as a percentage response to 10% (v/v) FBS (positive control).

Inhibition of cAMP accumulation

18 h after transfection, CHO-RXFP4 cells were trypsinized and seeded onto 96-well plates at a density of ~50,000 cells per well and incubated for 6–8 h in complete media to allow cell adhesion. Cells were then incubated with PT, EcPltAB, or control (serum-free DMEM/F-12 medium) for 18 h. On the day of experiment, we changed the medium to Hanks' balanced salt solution supplemented with 500 µM isobutylmethylxanthine, 5 mM HEPES, and 0.1% (w/v) BSA and equilibrated for 1 h at 37 °C. Cells were treated with INSL5 (100 nM) for 15 min, followed by 30 min of forskolin stimulation and then lysed with 100% ice-cold ethanol. Once ethanol has evaporated, cAMP was resuspended in 100 µl of lysis buffer containing 0.3% (v/v) Tween 20, 5 mM HEPES, and 0.1% (w/v) BSA. The amount of cAMP generated by forskolin and its inhibition by INSL5 was measured using a homogeneous time-resolved fluorescence resonance energy transfer LANCE cAMP kit (PerkinElmer Life Sciences) as per the manufacturer's protocol.

Figure 1.

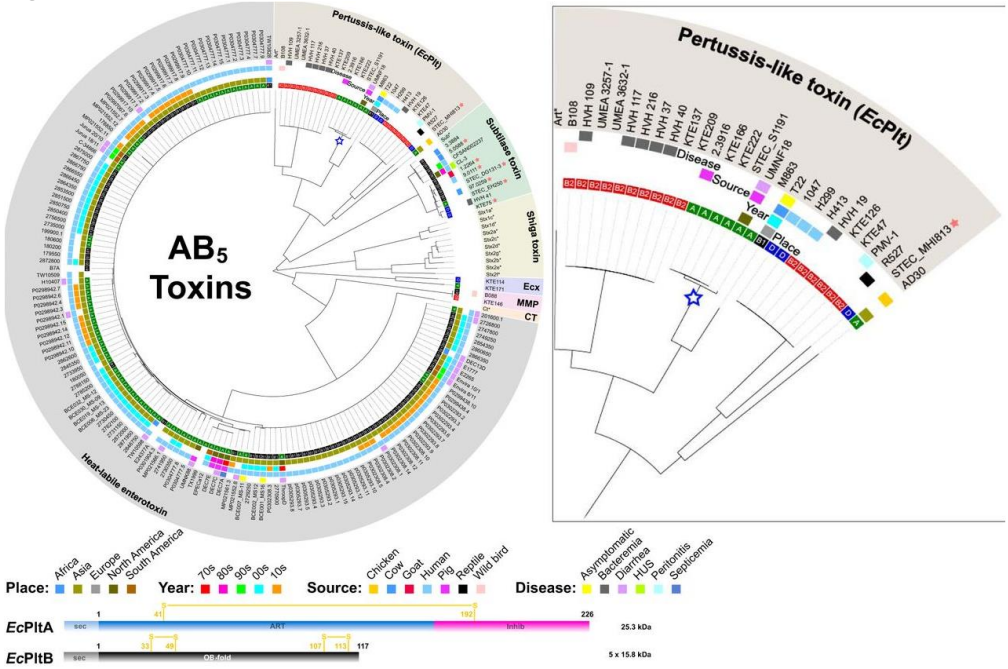

***E. coli* AB$_5$ toxins.** Shown is a cladogram of AB$_5$ toxin sequences identified in genome sequenced *E. coli* strains available on the NCBI database. Archetype sequences from the querying dataset are indicated with an *asterisk. E. coli* strains harboring more than one AB$_5$ group are indicated by a *red star*. The *inner circle* represents the *E. coli*phylogenetic groups (A, B1, B2, and D). Additional color-coded circles indicate the place, year, and source of each strain, as well as the associated infection (where known). Because Shiga toxigenic *E. coli* strains are over-represented in the NCBI database, only archetypical Shiga toxin variants are presented. The *Ec*PltA toxin focused on in this study is highlighted with a *blue star*. A schematic of the A and B subunit domain displayed with the positions of the intramolecular disulfides (*yellow*) and the inhibitory C terminus (*pink*) is at the bottom of the figure. *Inset,* an expanded view of the pertussis toxin branch. A complete overview of all Shiga toxin variants and their associated strains is presented in supplemental Fig. S1.

Figure 2

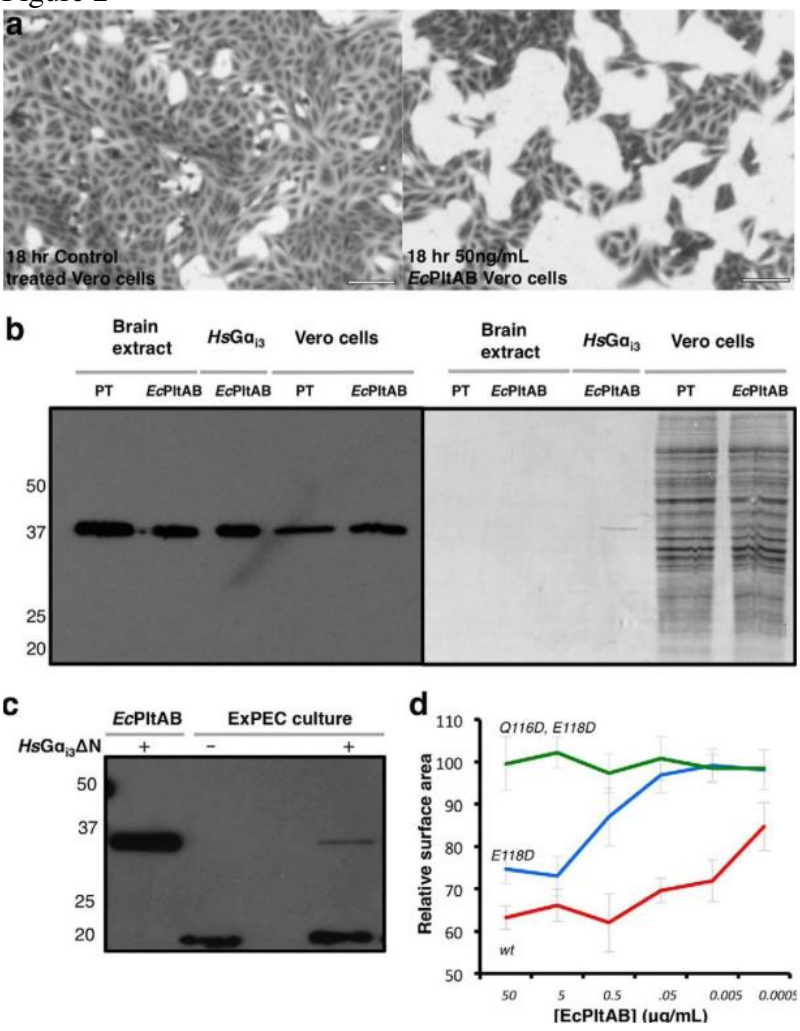

Cytotoxicity of recombinant *Ec*PltAB. 18 h after treatment with buffer or different concentrations of *Ec*PltAB, Vero cells were stained and imaged. *a,*representative images for untreated controls (*left*) and 50 ng/ml *Ec*PltAB (*right*) are shown. *b*, ADP-ribosyltransferase assays in which pertussis toxin or EcPltAB were used to modify different protein substrates, including trimeric G-protein extracts, recombinant human $G\alpha_{i3}$, or Vero cell lysates. Reactions at 37 °C were performed in the presence of biotin-NAD^+ and then quenched after 5 min, separated by SDS-PAGE, transferred to a Western blotting membrane, and imaged with either luminescence following streptactin-HRP exposure (*left*) or Coomassie (*right*). *c,* Western blottings showing the incubation of ExPEC culture medium with NAD^+-biotin with and without the presence of *Hs*$G\alpha_{i3}\Delta$N. *d*, Vero cells were imaged in a similar manner to those in *a* were monitored for the degree of cell growth relative to buffer controls following exposure to different concentrations of *Ec*PltAB or A subunit mutants. Surface area is calculated from the percentage of each image stained by crystal violet. Data represent the mean ± S.D. from three replicates

Figure 3

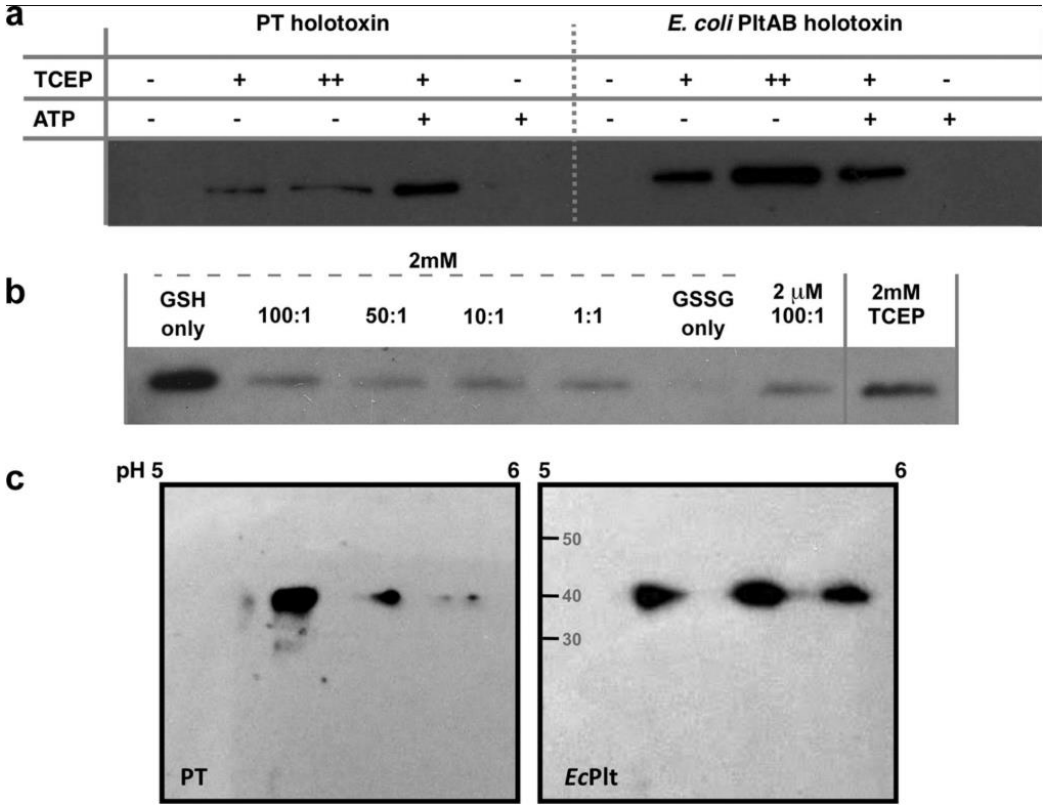

Activity assays for *Ec*PltAB. *a*, ADP-ribosyltransferase assays similar to those used in Fig. 2using biotinylated NAD^+ as a substrate to modify recombinant *Hs*Gαi3ΔN PT (*left*) and EcPltAB (*right*) holotoxins were monitored for activity for 5 min at 37 °C in the presence of 10 mM (+) or 100 mM (++) TCEP and with or without 10 mM ATP. *b*, *Ec*PltAB activation in the presence of different ratios of reduced (GSH) or oxidized (GSSG) glutathione within the ADP-ribosylation assay. *c,* 2D isoelectric focusing separation of different Ga_iisoforms isolated from bovine brain extract following treatment with *Ec*PltAB or PT indicate multiple Ga_i isoforms act as substrates

Figure 4

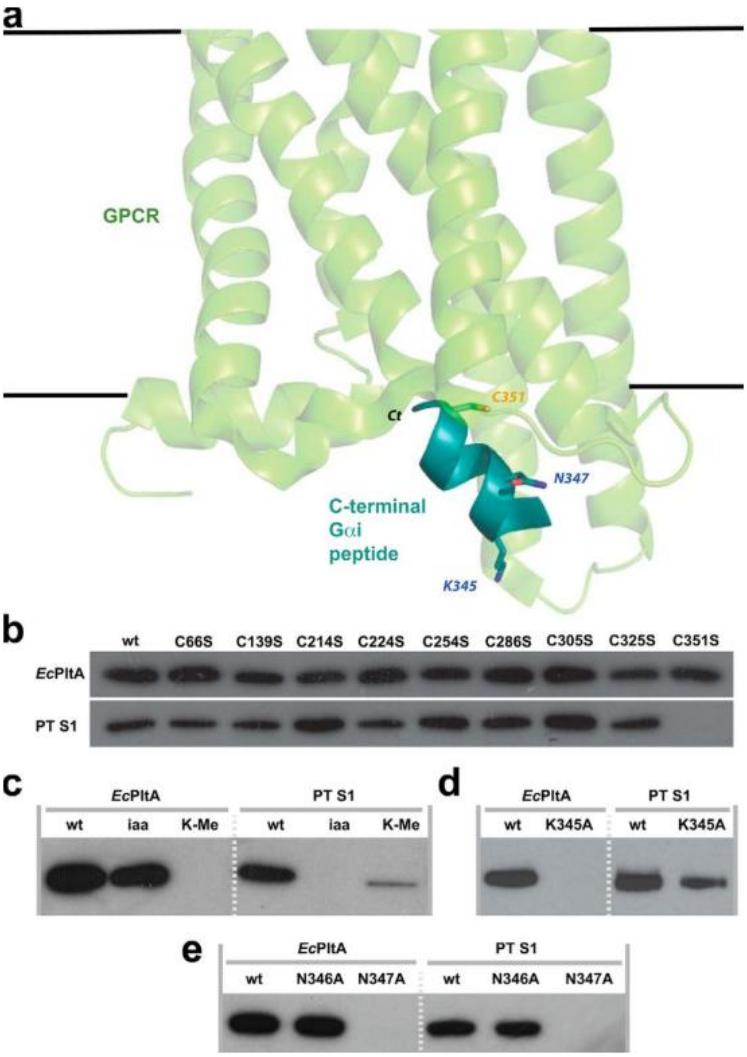

Proposed model of the pertussis-like toxins transfer target. *a,* structure of opsin in complex with the C terminus of transducin (Scheerer *et al.* (38), Protein Data Bank code 3DQD); their K345L mutant was reverted to lysine for this figure. $G\alpha_{i3}$ is shown in *teal*; the position of the C terminus and ADP-ribosylated residues discussed in text are shown. The plasma membrane and GPCR (*green*) are at the *top. b,* ADP-ribosyltransferase assays using *Ec*PltA or pertussis toxin in which potential acceptor cysteines within $G\alpha_{i3}\Delta N$ were mutated to serine; or *c,* following iodoacetamide and lysine methylation; *d*, mutation of Lys-345; or *e,* Asn-346 and Asn-347 to alanine

Figure 5

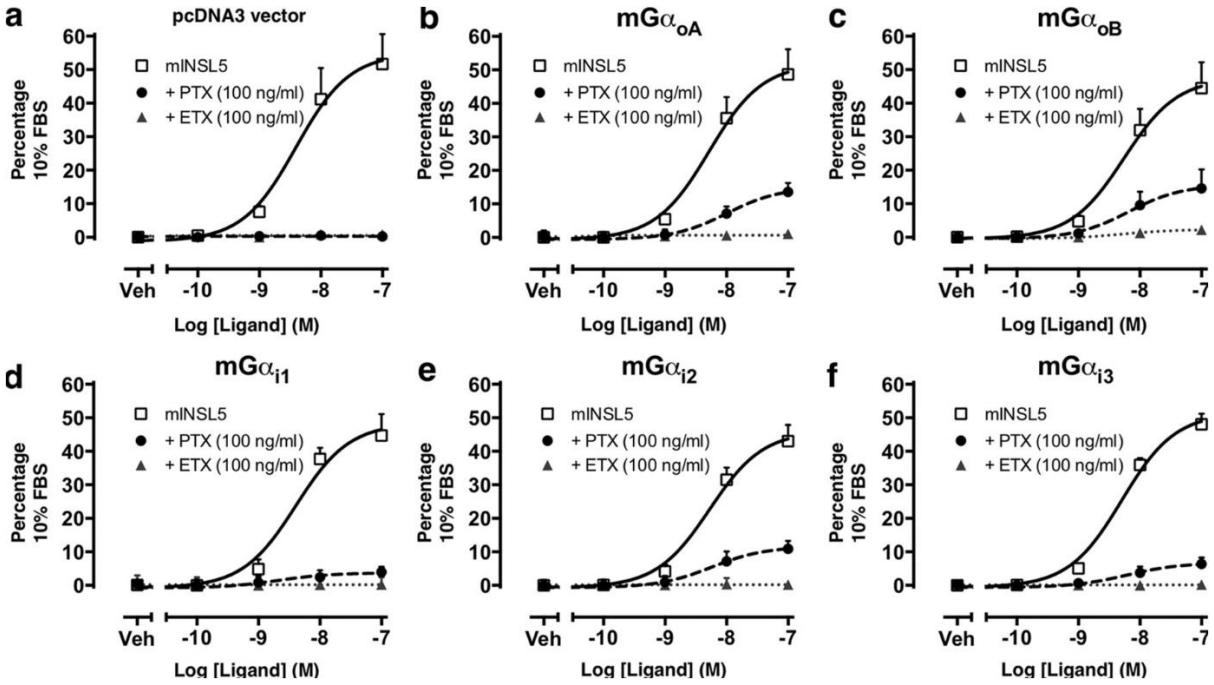

***Ec*PltAB disrupts G-protein-coupled signaling.** RXFP4 recruits $G_{i/o}$ α subunits upon ligand activation. PT pretreatment abolishes INSL5-stimulated ERK1/2 phosphorylation, and this is rescued to differing degrees by transfection of individual PT-insensitive $G_{i/o}$ mutants. *a,*Chinese hamster ovary-RXFP4 cells were transiently transfected with pcDNA3 vector control, or *b–f,* $G_{i/o}$ constructs carrying the C351I mutation ($mG\alpha_{oA}$, $mG\alpha_{oB}$, $mG\alpha_{i1}$, $mG\alpha_{i2}$, or $mG\alpha_{i3}$). Blockade of the response to PT but not *Ec*PltAB pretreatment was rescued by transfection of the mutant G-proteins. Cells were stimulated with mouse INSL5 alone (0.1 to 100 nM) or after pretreatment with PT (100 ng/ml) or *Ec*PltAB (100 ng/ml). Data points represent mean ± S.E. of three independent experiments and are expressed as the % response of the positive control (10% v/v FBS). *Veh*, vehicle

Figure 6

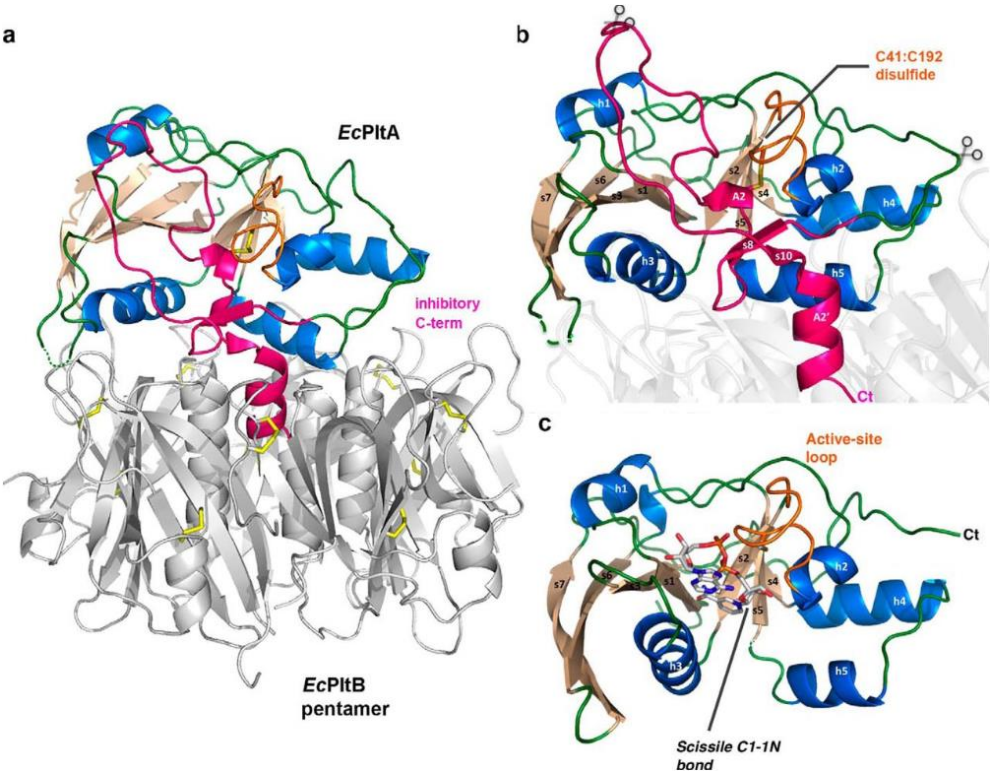

Activation mechanisms of *Ec*Plt and cholera toxin. *a,* schematic representation of the *Ec*PltAB holotoxin in which α-helices are colored *marine*, β-strands *wheat*, and loop regions *green*. The C-terminal A2 domain is highlighted in *pink* showing its interaction with the B subunits of the glycan-binding pentamer (*gray*). *b,* schematic representation highlighting the holotoxin's *Ec*PltA subunit. The conserved redox-sensing disulfide is labeled, and the rough position of the B-pentamer is shown as a partially transparent structure. Predicted potential proteolytic sites are shown with partially *transparent scissors*, and the C terminus is marked *Ct. c,* reduced active NAD^+ co-complex with all secondary structural elements labeled. The enzymatically cleaved *N*-glycosidic bond cleaved during the course of the reaction is *highlighted*

Figure 7

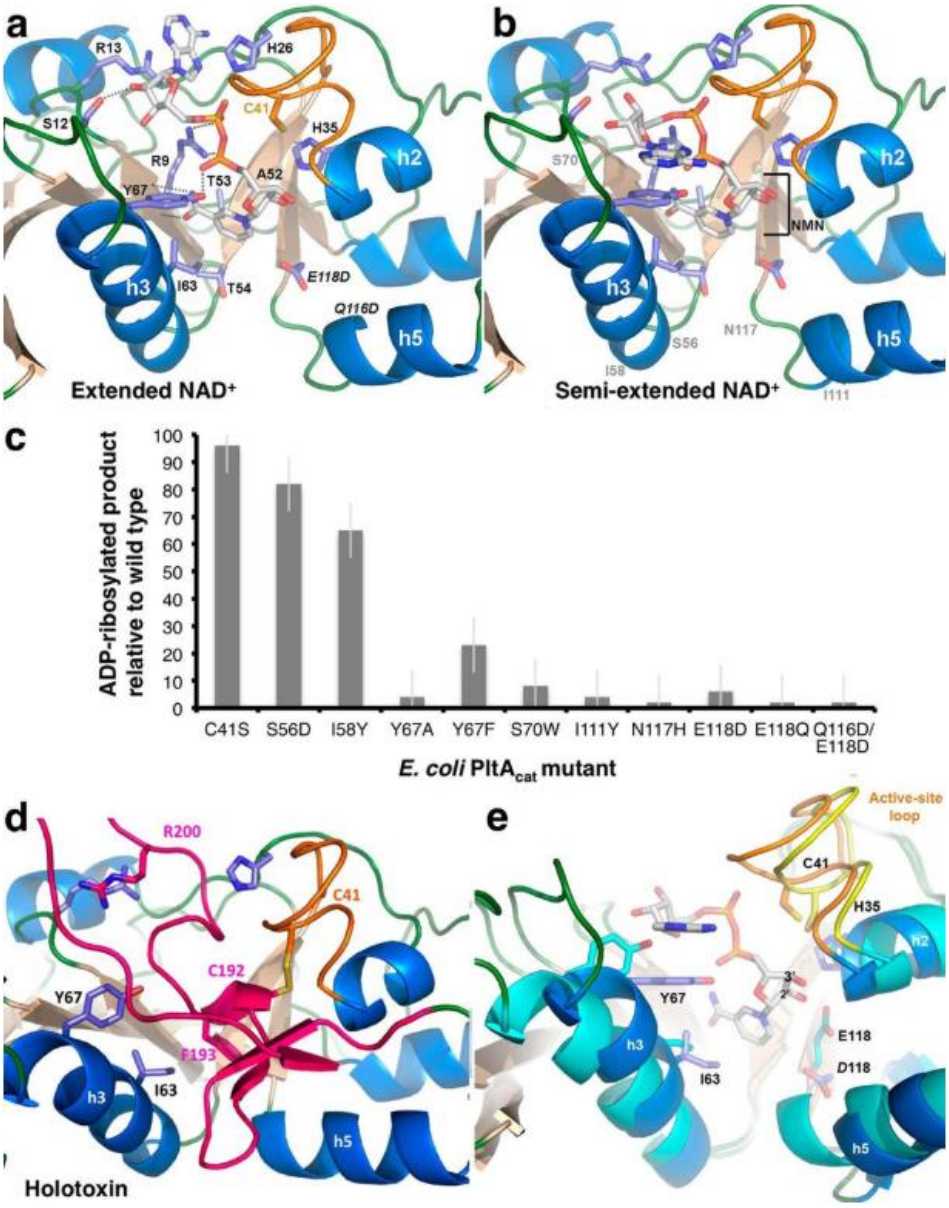

NAD$^+$-binding site of *Ec*PltA. *a*, structure of *Ec*PltA with NAD$^+$bound in the extended conformation; residues investigated for their role in binding and catalysis are labeled, as are the nicotinamide STS-clasp equivalent residues ^{52}ATT^{54}. *b,*structure of the semi-extended NAD$^+$ conformation, approximate position of occluding residue mutants are shown in *gray. c,* ADP-ribosyltransferase assay response relative to wild-type protein for various point mutants within the NAD$^+$-binding site. *Error bars*are the S.D. of three independent replicates. *d,* depiction of where the residues important for NAD$^+$ binding are located in the oxidized holotoxin and their interactions with the occluding A2 helix (*pink*). *e,* overlay highlighting the structural changes occurring during activation/NAD$^+$binding. The semi-extended NAD$^+$-bound structure (*blue helices* and *orange loop*) is compared with the oxidized holotoxin (*cyan helices* and *yellow loop*)

Table 1

Table 1

Data collection and refinement statistics

	*Ec*PltAB	*Ec*PltA1
Data collection		
Redox state	Oxidized	Reduced
Space group	$P6_5$	*P1*
Cell dimensions		
a, *b*, *c* (Å)	160.9, 160.9, 62.6	44.5, 55.7, 73.1
α, β, γ (°)	90.0, 90.0, 120.0	90.1, 104.1, 96.2
Resolution (Å)	49.4–2.35 (2.48–2.35)	70.8–1.80 (1.90–1.80)
R_{pim} [a]	4.1 (35.6)	6.6 (30)
I/σ_I	12.1 (2.1)	7.7 (2.6)
Completeness (%)	99.9 (99.7)	88.5 (87.7)
Total no. of observations	326,219 (45274)	91,849 (12898)
No. of unique observations	38,825 (5619)	55,479 (8027)
Multiplicity	8.4 (8.1)	1.7 (1.6)
Refinement statistics		
R_{factor} [b] (%)	19.2 (30.0)	18.1 (26.1)
R_{free} [c] (%)	25.5 (34.3)	22.7 (31.6)
No. of atoms		
Protein	6380	5591
Ligand	1 (PO_4)	176 (4 NAD^+, 2Na^+)
Water	64	598
Ramachandran plot (%)		
Most favored	94.0	97.5
Allowed region	6.0	2.5
Outlier	0.0	0.0
B-factors (Å^2)		
Protein	68.1	16.2
Root mean square deviation bonds (Å)	0.011	0.010
Root mean square deviation mangles (°)	1.37	1.18

- [a] $R_{p.i.m} = \Sigma_{hkl}(1/(N-1))^{1/2}\Sigma_i|I_{hkl,i} - \langle I_{hkl}\rangle|/\Sigma_{hkl}\langle I_{hkl}\rangle$.
- [b] $R_{factor} = (\Sigma||F_o| - |F_c||)/(\Sigma|F_o|)$ for all data except as indicated in Footnote *c*.
- [c] 5% of data was used for the R_{free} calculation.

REFERENCES

References

1. Kaper, J. B., Nataro, J. P., and Mobley, H. L. (2004) Pathogenic Escherichia coli. *Nature reviews. Microbiology* **2**, 123-140

2. Russo, T. A., and Johnson, J. R. (2000) Proposal for a new inclusive designation for extraintestinal pathogenic isolates of Escherichia coli: ExPEC. *The Journal of infectious diseases* **181**, 1753-1754

3. Wiles, T. J., Kulesus, R. R., and Mulvey, M. A. (2008) Origins and virulence mechanisms of uropathogenic Escherichia coli. *Experimental and molecular pathology* **85**, 11-19

4. Sixma, T. K., Pronk, S. E., Kalk, K. H., Wartna, E. S., van Zanten, B. A., Witholt, B., and Hol, W. G. (1991) Crystal structure of a cholera toxin-related heat-labile enterotoxin from E. coli. *Nature* **351**, 371-377

5. Zhang, R. G., Scott, D. L., Westbrook, M. L., Nance, S., Spangler, B. D., Shipley, G. G., and Westbrook, E. M. (1995) The three-dimensional crystal structure of cholera toxin. *Journal of molecular biology* **251**, 563-573

6. Paton, A. W., Srimanote, P., Talbot, U. M., Wang, H., and Paton, J. C. (2004) A new family of potent AB(5) cytotoxins produced by Shiga toxigenic Escherichia coli. *The Journal of experimental medicine* **200**, 35-46

7. Song, J., Gao, X., and Galan, J. E. (2013) Structure and function of the Salmonella Typhi chimaeric A(2)B(5) typhoid toxin. *Nature* **499**, 350-354

8. Katada, T., and Ui, M. (1982) ADP ribosylation of the specific membrane protein of C6 cells by islet-activating protein associated with modification of adenylate cyclase activity. *The Journal of biological chemistry* **257**, 7210-7216

9. Stein, P. E., Boodhoo, A., Armstrong, G. D., Cockle, S. A., Klein, M. H., and Read, R. J. (1994) The crystal structure of pertussis toxin. *Structure* **2**, 45-57

10. Beddoe, T., Paton, A. W., Le Nours, J., Rossjohn, J., and Paton, J. C. (2010) Structure, biological functions and applications of the AB5 toxins. *Trends in biochemical sciences* **35**, 411-418

11. Byres, E., Paton, A. W., Paton, J. C., Lofling, J. C., Smith, D. F., Wilce, M. C., Talbot, U. M., Chong, D. C., Yu, H., Huang, S., Chen, X., Varki, N. M., Varki, A., Rossjohn, J., and Beddoe, T. (2008) Incorporation of a non-human glycan mediates human susceptibility to a bacterial toxin. *Nature* **456**, 648-652

12. Ng, N. M., Littler, D. R., Paton, A. W., Le Nours, J., Rossjohn, J., Paton, J. C., and Beddoe, T. (2013) EcxAB is a founding member of a new family of metalloprotease AB5 toxins with a hybrid cholera-like B subunit. *Structure* **21**, 2003-2013

13. Katada, T. (2012) The inhibitory G protein G(i) identified as pertussis toxin-catalyzed ADPribosylation. *Biological & pharmaceutical bulletin* **35**, 2103-2111

14. Locht, C., Lobet, Y., Feron, C., Cieplak, W., and Keith, J. M. (1990) The role of cysteine 41 in the enzymatic activities of the pertussis toxin S1 subunit as investigated by site-directed mutagenesis. *The Journal of biological chemistry* **265**, 4552-4559

15. O'Neal, C. J., Jobling, M. G., Holmes, R. K., and Hol, W. G. (2005) Structural basis for the activation of cholera toxin by human ARF6-GTP. *Science* **309**, 1093-1096

16. Saitoh, M., Tanaka, K., Nishimori, K., Makino, S., Kanno, T., Ishihara, R., Hatama, S., Kitano, R., Kishima, M., Sameshima, T., Akiba, M., Nakazawa, M., Yokomizo, Y., and Uchida, I. (2005) The artAB genes encode a putative ADP-ribosyltransferase toxin homologue associated with Salmonella enterica serovar Typhimurium DT104. *Microbiology* **151**, 3089-3096

17. Uchida, I., Ishihara, R., Tanaka, K., Hata, E., Makino, S., Kanno, T., Hatama, S., Kishima, M., Akiba, M., Watanabe, A., and Kubota, T. (2009) Salmonella enterica serotype Typhimurium DT104 ArtA-dependent modification of pertussis toxin-sensitive G proteins in the presence of [32P]NAD. *Microbiology* **155**, 3710-3718

18. Ng, N., Littler, D., Le Nours, J., Paton, A. W., Paton, J. C., Rossjohn, J., and Beddoe, T. (2013) Cloning, expression, purification and preliminary X-ray diffraction studies of a novel AB toxin. *Acta crystallographica. Section F, Structural biology and crystallization communications* **69**, 912-915

19. Hewlett, E. L., Sauer, K. T., Myers, G. A., Cowell, J. L., and Guerrant, R. L. (1983) Induction of a novel morphological response in Chinese hamster ovary cells by pertussis toxin. *Infection and immunity* **40**, 1198-1203

20. Katada, T., and Ui, M. (1982) Direct modification of the membrane adenylate cyclase system by islet-activating protein due to ADP-ribosylation of a membrane protein. *Proceedings of the National Academy of Sciences of the United States of America* **79**, 3129-
3133

21. Hausman, S. Z., Cherry, J. D., Heininger, U., Wirsing von Konig, C. H., and Burns, D. L. (1996) Analysis of proteins encoded by the ptx and ptl genes of Bordetella bronchiseptica and Bordetella parapertussis. *Infection and immunity* **64**, 4020-4026

22. Wang, H., Paton, J. C., Herdman, B. P., Rogers, T. J., Beddoe, T., and Paton, A. W. (2013) The B subunit of an AB5 toxin produced by Salmonella enterica serovar Typhi up-regulates chemokines, cytokines, and adhesion molecules in human macrophage, colonic epithelial, and brain microvascular endothelial cell lines. *Infection and immunity* **81**, 673-683

23. Antoine, R., Tallett, A., van Heyningen, S., and Locht, C. (1993) Evidence for a catalytic role of glutamic acid 129 in the NAD-glycohydrolase activity of the pertussis toxin S1 subunit. *The Journal of biological chemistry* **268**, 24149-24155

24. Kaslow, H. R., Lim, L. K., Moss, J., and Lesikar, D. D. (1987) Structure-activity analysis of the activation of pertussis toxin. *Biochemistry* **26**, 123-127

25. Hazes, B., Boodhoo, A., Cockle, S. A., and Read, R. J. (1996) Crystal structure of the pertussis toxin-ATP complex: a molecular sensor. *Journal of molecular biology* **258**, 661-671

26. Hoshino, S., Kikkawa, S., Takahashi, K., Itoh, H., Kaziro, Y., Kawasaki, H., Suzuki, K., Katada, T., and Ui, M. (1990) Identification of sites for alkylation by N-ethylmaleimide and pertussis toxin-catalyzed ADP-ribosylation on GTP-binding proteins. *FEBS letters* **276**, 227-231

27. Avigan, J., Murtagh, J. J., Jr., Stevens, L. A., Angus, C. W., Moss, J., and Vaughan, M. (1992) Pertussis toxin-catalyzed ADP-ribosylation of G(o) alpha with mutations at the carboxyl terminus. *Biochemistry* **31**, 7736-7740

28. Freissmuth, M., and Gilman, A. G. (1989) Mutations of GS alpha designed to alter the reactivity of the protein with bacterial toxins. Substitutions at ARG187 result in loss of GTPase ac tivity. *The Journal of biological chemistry* **264**, 21907-21914

29. Bathgate, R. A., Halls, M. L., van der Westhuizen, E. T., Callander, G. E., Kocan, M., and Summers, R. J. (2013) Relaxin family peptides and their receptors. *Physiological reviews*
93, 405-480

30. O'Neal, C. J., Amaya, E. I., Jobling, M. G., Holmes, R. K., and Hol, W. G. (2004) Crystal structures of an intrinsically active cholera toxin mutant yield insight into the toxin activation mechanism. *Biochemistry* **43**, 3772-3782

31. Kuppuraj, G., Sargsyan, K., Hua, Y. H., Merrill, A. R., and Lim, C. (2011) Linking distinct conformations of nicotinamide adenine dinucleotide with protein fold/function. *The journal of physical chemistry. B* **115**, 7932-7939

32. Tsurumura, T., Tsumori, Y., Qiu, H., Oda, M., Sakurai, J., Nagahama, M., and Tsuge, H. (2013) Arginine ADP-ribosylation mechanism based on structural snapshots of iota-toxin. *Proceedings of the National Academy of Sciences of the United States of America* **110**, 4267-4272

33. Tsuge, H., and Tsurumura, T. (2015) Reaction Mechanism of Mono-ADPRibosyltransferase Based on Structures of the Complex of Enzyme and Substrate Protein. *Current topics in microbiology and immunology* **384**, 69-87

34. Menetrey, J., Flatau, G., Boquet, P., Menez, A., and Stura, E. A. (2008) Structural basis for the NAD-hydrolysis mechanism and the ARTT-loop plasticity of C3 exoenzymes. *Protein science : a publication of the Protein Society* **17**, 878-886

35. Xu, Y., Barbancon-Finck, V., and Barbieri, J. T. (1994) Role of histidine 35 of the S1 subunit of pertussis toxin in the ADP-ribosylation of transducin. *The Journal of biological chemistry* **269**, 9993-9999

36. Cummings, M. D., Hart, T. N., and Read, R. J. (1998) Fragment-based modeling of NAD binding to the catalytic subunits of diphtheria and pertussis toxins. *Proteins* **31**, 282-298

37. Messner, S., Altmeyer, M., Zhao, H., Pozivil, A., Roschitzki, B., Gehrig, P., Rutishauser, D., Huang, D., Caflisch, A., and Hottiger, M. O. (2010) PARP1 ADP-ribosylates lysine residues of the core histone tails. *Nucleic acids research* **38**, 6350-6362

38. Scheerer, P., Park, J. H., Hildebrand, P. W., Kim, Y. J., Krauss, N., Choe, H. W., Hofmann, K. P., and Ernst, O. P. (2008) Crystal structure of opsin in its G-protein-interacting conformation. *Nature* **455**, 497-502

39. Graf, R., Codina, J., and Birnbaumer, L. (1992) Peptide inhibitors of ADP-ribosylation by pertussis toxin are substrates with affinities comparable to those of the trimeric GTP-binding proteins. *Molecular pharmacology* **42**, 760-764

40. Akhter Hossain, M., Bathgate, R. A., Kong, C. K., Shabanpoor, F., Zhang, S., Haugaard-Jonsson, L. M., Rosengren, K. J., Tregear, G. W., and Wade, J. D. (2008) Synthesis, conformation, and activity of human insulin-like peptide 5 (INSL5). *Chembiochem : a European journal of chemical biology* **9**, 1816-1822

41. Bergan, J., Dyve Lingelem, A. B., Simm, R., Skotland, T., and Sandvig, K. (2012) Shiga toxins. *Toxicon : official journal of the International Society on Toxinology* **60**, 1085-1107

42. Chong, D. C., Paton, J. C., Thorpe, C. M., and Paton, A. W. (2007) Clathrin-dependent trafficking of subtilase cytotoxin, a novel AB(5) toxin that targets the endoplasmic reticulum chaperone BiP. *Cell Microbiol*

43. Sanchez, J., and Holmgren, J. (2008) Cholera toxin structure, gene regulation and pathophysiological and immunological aspects. *Cell Mol Life Sci* **65**, 1347-1360

44. Pearson, W. R., and Lipman, D. J. (1988) Improved tools for biological sequence comparison. *Proceedings of the National Academy of Sciences of the United States of America* **85**, 2444-2448

45. Chenna, R., Sugawara, H., Koike, T., Lopez, R., Gibson, T. J., Higgins, D. G., and Thompson, J. D. (2003) Multiple sequence alignment with the Clustal series of programs. *Nucleic acids research* **31**, 3497-3500

46. Clermont, O., Bonacorsi, S., and Bingen, E. (2000) Rapid and simple determination of the Escherichia coli phylogenetic group. *Applied and environmental microbiology* **66**, 4555-4558

47. Escobar-Paramo, P., Le Menac'h, A., Le Gall, T., Amorin, C., Gouriou, S., Picard, B., Skurnik, D., and Denamur, E. (2006) Identification of forces shaping the commensal Escherichia coli genetic structure by comparing animal and human isolates. *Environmental microbiology* **8**, 1975-1984

48. Wirth, T., Falush, D., Lan, R., Colles, F., Mensa, P., Wieler, L. H., Karch, H., Reeves, P. R., Maiden, M. C., Ochman, H., and Achtman, M. (2006) Sex and virulence in Escherichia coli: an evolutionary perspective. *Mol Microbiol* **60**, 1136-1151

49. Adams, P. D., Afonine, P. V., Bunkoczi, G., Chen, V. B., Davis, I. W., Echols, N., Headd, J. J., Hung, L. W., Kapral, G. J., Grosse-Kunstleve, R. W., McCoy, A. J., Moriarty, N. W., Oeffner, R., Read, R. J., Richardson, D. C., Richardson, J. S., Terwilliger, T. C., and Zwart, P. H. (2010) PHENIX: a comprehensive Python-based system for macromolecular structure solution. *Acta crystallographica. Section D, Biological crystallography* **66**, 213-221

50. McCoy, A. J., Grosse-Kunstleve, R. W., Adams, P. D., Winn, M. D., Storoni, L. C., and Read, R. J. (2007) Phaser crystallographic software. *Journal of applied crystallography* **40**, 658-674

51. Emsley, P., Lohkamp, B., Scott, W. G., and Cowtan, K. (2010) Features and development of Coot. *Acta crystallographica. Section D, Biological crystallography* **66**, 486-501

52. Samson, A. L., Knaupp, A. S., Kass, I., Kleifeld, O., Marijanovic, E. M., Hughes, V. A., Lupton, C. J., Buckle, A. M., Bottomley, S. P., and Medcalf, R. L. (2014) Oxidation of an exposed methionine instigates the aggregation of glyceraldehyde-3-phosphate dehydrogenase. *The Journal of biological chemistry* **289**, 26922-26936

53. Cox, J., and Mann, M. (2008) MaxQuant enables high peptide identification rates, individualized p.p.b.-range mass accuracies and proteome-wide protein quantification. *Nature biotechnology* **26**, 1367-1372